https://doi.org/10.1016/j.apm.2020.10.008

This is the Pre-Published Version.

Mathematical Modeling of Linearly-elastic Non-prestrained Cables Based on a Local Reference Frame

H. B. Tang[a], Y. Han[a], H. Fu[b], B. G. Xu[c,*]

[a] *School of Automobile, Chang'an University, Xi'an, China*
[b] *Department of Mathematics and Information Technology, The Education University of Hong Kong, Hong Kong*
[c] *Institute of Textiles and Clothing, The Hong Kong Polytechnic University, Hung Hom, Kowloon, Hong Kong*

Abstract

Cables are widely used and serve different purposes in engineering. This paper aims to formulate a general dynamic model on extensible non–prestrained cables under external forces. In terms of the Hamilton's principle, the governing equation and boundary conditions are achieved according to the variation of action integral. Meanwhile, the local reference frame of the cable curve is illustrated which is composed of four vectors. In the presented model, it is shown that the external force along the binormal direction could not be balanced by the internal tensile force of the cable itself. And the curved cable will result in an elastic force in the normal direction which is in a linear relationship with the curvature of the cable. Further, this approach is applied to cables under uniformly distributed loads or self–weights. The contours and internal tensile forces of the cables are figured out by means of numerical methods. The developed model is evaluated by means of experimental data in published literature. The good agreement between the numerical and experimental results shows that the presented method is feasible in theory.

Keywords: Extensible non–prestrained cable, The Hamilton's principle, Local reference frame, Mathematical modeling

*Corresponding author.
Email address: tcxubg@polyu.edu.hk (B. G. Xu)

© 2020. This manuscript version is made available under the CC-BY-NC-ND 4.0 license http://creativecommons.org/licenses/by-nc-nd/4.0/.

1. Introduction

Cables or strings are widely used in various sections of engineering. Suspension bridges are a type of bridge in which suspension cables are anchored at each end of the bridge and carry the majority of load. Cable–stayed bridges are similar to suspension bridges, but the cables are used to directly attach the roadway to a tower which bears the weight alone. Further, pantograph–catenary systems are important parts of electrical trains, which could supply uninterrupted power to the running trains. The catenary system generally consists of a message wire and a contact wire. The message wire is suspended by brackets and connected to the contact wire. The catenary system is dynamically interacted with the pantograph. In textile engineering, yarns are as extensible cables of which the quality is heavily influenced by the manufacture process. On the applications of cables, the fundamental theoretical model is of significance to understand the dynamic behavior of cables.

On cable dynamics, Perkins and Mote[1] probed a traveling cable passing through two fixed eyelets, and the nonlinear governing equations of the sagged cable were derived in terms of the Hamilton's principle. Further, elastic cables which are suspended between two–level supports and subject to planar excitation were investigated by Lee and Perkins[2]. Luongo and Piccardo[3] studied the dynamic responses of an elastic cable suspended between two fixed supports considering wind flows perpendicular to the plane of the cable. The investigations on mathematical modeling and nonlinear vibrations of suspended cables were reviewed by Rega[4]. Luongo et al.[5] developed a linear elastic model of curved and prestressed beams of which the self–weight of cables and static wind forces are considered. The equation of motion of cables is simplified by a magnitude order analysis. In those models, the governing equations of suspended elastic cables are achieved in the Frenet frame of cables. Meanwhile, initial configurations of cables are given to reckon the strain of cables.

In bridge engineering, Kang et al.[6] presented a nonlinear dynamic model

of cable–stayed bridges. In that work, a scheme employing double–cable–stayed shallow arches is proposed. Hashemi et al.[7] studied the dynamic responses of a cable–stayed bridge under the blast load in terms of the finite element method (FEM). Song et al.[8] probed a cable–stayed bridge subjected to moving loads, and the nonlinearity of stayed cables is considered. Xie et al.[9] studied the static and dynamic behavior of cable–stayed bridges. In the model, carbon fiber reinforced polymer cables are used and simulated by the FEM. Moreover, nonlinear seismic responses of a cable-stayed bridge were evaluated by Han et al.[10] and Javanmardi et al.[11] considering the pre-strained cables.

Further, the thermal effects on suspended cables were investigated in references [12, 13, 14], which result in more complicated models. Wei et al.[15] developed a nonlinear model of cable–stayed beams, and the bifurcation and chaos of the model are investigated.

On pantograph–catenary systems, Song et al.[16] investigated wind-induced vibrations of the high speed catenary and dynamic behavior of pantograph–catenary systems, and nonlinearity of the catenary model is considered. Antunes et al.[17] studied the pantograph–catenary interaction in curved railway tracks. By using the FEM, Euler–Bernoulli beam elements are used to model the catenary. FEM models of pantograph–catenary systems were developed by Gregori et al.[18] and Gregori et al.[19] which could notably improve the effectiveness of numerical computations. The contact forces in pantograph–catenary systems were researched by Song et al.[20] and Nåvik et al.[21] Further, Song et al.[22] presented an analytical model to study the wave propagation property in railway catenary systems. In that model, the governing equation of a tensioned cable without bending stiffness is employed. Moreover, Song et al.[23] presented a nonlinear model of the high speed catenary system, and nonlinear cable elements are used to obtain the deformed catenary system.

In addition, Guo et al.[24, 25] studied cable–support coupled systems by using an asymptotic expansion technique, and non-dimensional cable dynamic equations are used to obtain the dynamic responses of the coupled system. Nonlinear models composed of two cantilever beams connected by a suspended

cable were investigated by Gattulli et al.[26, 27] In those models, the flexible cables under self-weight are considered.

In textile engineering, ring spinning has been the major manufacturing system for spun yarns. Yarn balloons generated in the spinning machine affect the manufacture process and quality of yarn significantly. Fraser[28] presented a comprehensive analysis on the governing equations of yarn balloons in theoretical and numerical ways. Tang et al.[29] investigated yarn behavior in a modified ring spinning system. The numerical results show that the yarn paths have several classic modes under different yarn tensions. Yin et al.[30] developed a theoretical model of yarn dynamics in a generalized twisting system in which the twisting element is a moving rigid cylinder. Hossain et al.[31] studied the distribution of yarn tensions and balloon shapes influenced by spindle speeds. Besides, Xu and Tao[32] formulated an integrated dynamic model to probe the yarn twist propagation in rotor spinning.

In previous research on yarn dynamics, yarns are assumed to be inextensible in theory. Nevertheless, the extension of yarns under tensile forces is definitely occurred in practice. Yarns are a kind of extensible cable with little bending stiffness, which could not bear the bending moments.

In this work, a dynamic model of extensible non–prestrained cables will be developed in terms of the Hamilton's principle. The governing equation of the cable is formulated in a local reference frame, which is different from the traditional Frenet frame.

The remainder of the paper is arranged as follows. Section 2 presents the procedure of theoretical modeling and characteristics of the model. Then applications of the developed model are exhibited in Section 3. Further, the presented model is evaluated by using the experimental results in Section 4. Finally, the work is summarized in the last section.

2. Theory

In this section, the dynamic model of extensible non–prestrained cables is constructed in theory, and the characteristics of the governing equation are addressed.

In the first place, assumptions on cables are made for the following mathematical modeling.

(1) The cable can only be elongated and can not be shrunk, and its material is linear elastic.

(2) The cable can not bear bending moments and can sustain only tensile forces.

(3) The contour of the cable is sufficiently smooth.

Here assumption (2) means the bending moments will not induce extra deformation energies to the cable.

2.1. Dynamic modeling

The dynamic model considered in the work could be depicted in Fig. 1. The extensible cable in a coordinate system is positioned by vector $\boldsymbol{R}(s,t)$ where variables s and t are the arc length of the cable and time.

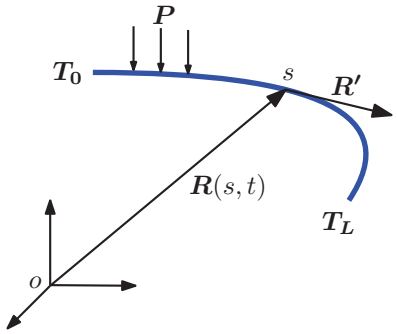

Figure 1: The schematic of the extensible non–prestained cable.

In differential geometry[33], an important relationship is given by

$$\boldsymbol{R}' \cdot \boldsymbol{R}' = 1, \tag{1}$$

where the superscript prime is used to indicate the derivative with respect to arc length s, and the operator dot means the dot product of two vectors. Note that the relationship implies that the arc is inextensible.

Consider a segment of cable in the range $[s, s + ds]$, the length of which is ds. The elongation of the arc could be approximated to

$$\boldsymbol{R}(s + ds, t) - \boldsymbol{R}(s, t) = \boldsymbol{R'}(s, t)ds. \tag{2}$$

If the cable is extensible, its axial strain is reached as

$$\epsilon = \sqrt{\boldsymbol{R'} \cdot \boldsymbol{R'}} - 1. \tag{3}$$

While the cable is inextensible, its axial strain will equal zero (see Eq. (1)).

In terms of the stress–strain relationship $\sigma = E\epsilon$, the elastic potential energy U of the system could be given by

$$U = \int_0^L \frac{1}{2} EA\epsilon^2 ds, \tag{4}$$

where E and A are the elastic modulus and cross-sectional area of the cable. Those two parameters are assumed to be constants in the work. And L is the length of the cable.

Moreover, the kinetic energy T of the system is read as

$$T = \int_0^L \frac{1}{2} m\dot{\boldsymbol{R}} \cdot \dot{\boldsymbol{R}} ds, \tag{5}$$

where m is the linear density of the cable. In the work, the dot or dots above a function denote the differentiation with respect to time t.

The work W induced by the distributed force $\boldsymbol{P}(s)$ and tensile forces on boundaries of the cable can be expressed as

$$W = \int_0^L \boldsymbol{P}(s) \cdot \boldsymbol{R}(s, t)ds + \boldsymbol{T}_L \cdot \boldsymbol{R}(L, t) - \boldsymbol{T}_0 \cdot \boldsymbol{R}(0, t), \tag{6}$$

where $\boldsymbol{T}_0$ and $\boldsymbol{T}_L$ are the tensile forces at the two endpoints of the cable.

In terms of the Hamilton's principle, the variation of the action integral from time $t0$ to $t1$ will be zero for a dynamic system. Thus it yields the relationship

$$\int_{t0}^{t1} \delta T - \delta U + \delta W dt = 0, \tag{7}$$

where the operator δ stands for the variation of a functional.

Considering the variation of the kinetic energy, we could obtain

$$\begin{aligned}\int_{t0}^{t1}\delta T dt &= \int_{t0}^{t1}\delta(\int_0^L \frac{1}{2}m\dot{\boldsymbol{R}}\cdot\dot{\boldsymbol{R}}ds)dt = \int_{t0}^{t1}\int_0^L m\dot{\boldsymbol{R}}\cdot\delta\dot{\boldsymbol{R}}dsdt \\ &= \int_0^L\int_{t0}^{t1}\frac{d(m\dot{\boldsymbol{R}}\cdot\delta\boldsymbol{R})}{dt}dtds - \int_{t0}^{t1}\int_0^L m\ddot{\boldsymbol{R}}\cdot\delta\boldsymbol{R}dsdt \\ &= \int_0^L m\dot{\boldsymbol{R}}\cdot\delta\boldsymbol{R}\Big|_{t0}^{t1}ds - \int_{t0}^{t1}\int_0^L m\ddot{\boldsymbol{R}}\cdot\delta\boldsymbol{R}dsdt. \end{aligned} \tag{8}$$

Assume that the cable has deterministic shapes at time $t0$ and $t1$. That means the variation of the cable curve will vanished at that time and the variation of the kinetic energy could be simplified as

$$\int_{t0}^{t1}\delta T dt = -\int_{t0}^{t1}\int_0^L m\ddot{\boldsymbol{R}}\cdot\delta\boldsymbol{R}dsdt. \tag{9}$$

The variation of the potential energy is given by

$$\begin{aligned}&\int_{t0}^{t1}\delta(\int_0^L\frac{1}{2}EA\epsilon^2 ds)dt = \int_{t0}^{t1}\int_0^L EA\epsilon\delta\epsilon dsdt \\ &= \int_{t0}^{t1}\int_0^L EA(\sqrt{\boldsymbol{R'}\cdot\boldsymbol{R'}}-1)\frac{\boldsymbol{R'}}{\sqrt{\boldsymbol{R'}\cdot\boldsymbol{R'}}}\cdot\delta\boldsymbol{R'}dsdt \\ &= \int_{t0}^{t1}EA(\sqrt{\boldsymbol{R'}\cdot\boldsymbol{R'}}-1)\frac{\boldsymbol{R'}}{\sqrt{\boldsymbol{R'}\cdot\boldsymbol{R'}}}\cdot\delta\boldsymbol{R}\Big|_0^L dt \\ &\quad -\int_{t0}^{t1}\int_0^L EA\left\{\frac{\boldsymbol{R''}\cdot\boldsymbol{R'}}{(\sqrt{\boldsymbol{R'}\cdot\boldsymbol{R'}})^3}\boldsymbol{R'}+(\sqrt{\boldsymbol{R'}\cdot\boldsymbol{R'}}-1)\frac{\boldsymbol{R''}}{\sqrt{\boldsymbol{R'}\cdot\boldsymbol{R'}}}\right\}\cdot\delta\boldsymbol{R}dsdt. \end{aligned} \tag{10}$$

The variation of the work caused by external forces is given by

$$\int_{t0}^{t1}\delta W dt = \int_{t0}^{t1}\int_0^L \boldsymbol{P}\cdot\delta\boldsymbol{R}ds + \boldsymbol{T}_L\cdot\delta\boldsymbol{R}(L,t) - \boldsymbol{T}_0\cdot\delta\boldsymbol{R}(0,t)dt. \tag{11}$$

In terms of Eq. (7), the final variation equation of the dynamic system could be achieved as

$$\begin{aligned}&\int_{t0}^{t1}\int_0^L\left\{-m\ddot{\boldsymbol{R}}+EA\left\{\frac{\boldsymbol{R''}\cdot\boldsymbol{R'}}{(\sqrt{\boldsymbol{R'}\cdot\boldsymbol{R'}})^3}\boldsymbol{R'}+(\sqrt{\boldsymbol{R'}\cdot\boldsymbol{R'}}-1)\frac{\boldsymbol{R''}}{\sqrt{\boldsymbol{R'}\cdot\boldsymbol{R'}}}\right\}+\boldsymbol{P}\right\}\cdot\delta\boldsymbol{R}ds \\ &-EA(\sqrt{\boldsymbol{R'}\cdot\boldsymbol{R'}}-1)\frac{\boldsymbol{R'}}{\sqrt{\boldsymbol{R'}\cdot\boldsymbol{R'}}}\cdot\delta\boldsymbol{R}\Big|_0^L+\boldsymbol{T}_L\cdot\delta\boldsymbol{R}(L,t)-\boldsymbol{T}_0\cdot\delta\boldsymbol{R}(0,t)dt=0. \end{aligned} \tag{12}$$

Next, considering the arbitrariness of variation of the cable shapes, the governing equation of the system could be formulated as

$$m\ddot{\boldsymbol{R}} - EA\frac{\boldsymbol{R''}\cdot\boldsymbol{R'}}{(\sqrt{\boldsymbol{R'}\cdot\boldsymbol{R'}})^3}\boldsymbol{R'} - EA(\sqrt{\boldsymbol{R'}\cdot\boldsymbol{R'}}-1)\frac{\boldsymbol{R''}}{\sqrt{\boldsymbol{R'}\cdot\boldsymbol{R'}}} = \boldsymbol{P}. \tag{13}$$

And the corresponding boundary conditions are given by

$$\begin{aligned} &-\left\{EA(\sqrt{\boldsymbol{R'}\cdot\boldsymbol{R'}}-1)\frac{\boldsymbol{R'}}{\sqrt{\boldsymbol{R'}\cdot\boldsymbol{R'}}}\Big|_L - \boldsymbol{T}_L\right\}\cdot\delta\boldsymbol{R}(L,t) \\ &\quad+\left\{EA(\sqrt{\boldsymbol{R'}\cdot\boldsymbol{R'}}-1)\frac{\boldsymbol{R'}}{\sqrt{\boldsymbol{R'}\cdot\boldsymbol{R'}}}\Big|_0 - \boldsymbol{T}_0\right\}\cdot\delta\boldsymbol{R}(0,t) = 0. \end{aligned} \tag{14}$$

Note that the work performed by force $\boldsymbol{P}(s)$ is assumed to be positive and the force will be negative in the case of negative work.

In addition, it should be emphasized that vectors $\boldsymbol{R'}$ and $\boldsymbol{R''}$ are not orthogonal to each other, which will be discussed in the next subsection.

2.2. Characteristics of the model

In what follows, the local reference frame of spatial curves is studied. According to Eq. (2), the unit tangent $\boldsymbol{t}$ of the curve $\boldsymbol{R}(s,t)$ could be written as

$$\boldsymbol{t} = \frac{\boldsymbol{R'}}{\sqrt{\boldsymbol{R'}\cdot\boldsymbol{R'}}}. \tag{15}$$

In other words, that means the relationship

$$\frac{\boldsymbol{R'}}{\sqrt{\boldsymbol{R'}\cdot\boldsymbol{R'}}}\cdot\frac{\boldsymbol{R'}}{\sqrt{\boldsymbol{R'}\cdot\boldsymbol{R'}}} = 1. \tag{16}$$

Then, differentiating the both hand sides of Eq. (16) with respect to s will yield

$$\frac{\boldsymbol{R'}}{\sqrt{\boldsymbol{R'}\cdot\boldsymbol{R'}}}\cdot\left\{\frac{\boldsymbol{R''}}{\sqrt{\boldsymbol{R'}\cdot\boldsymbol{R'}}} - \frac{(\boldsymbol{R'}\cdot\boldsymbol{R''})\boldsymbol{R'}}{(\boldsymbol{R'}\cdot\boldsymbol{R'})\sqrt{\boldsymbol{R'}\cdot\boldsymbol{R'}}}\right\} = 0. \tag{17}$$

This equation is an identity which could be proved by expanding it. Meanwhile, the normal $\boldsymbol{n}$ of the curve could be written as

$$\boldsymbol{n} = \frac{\boldsymbol{R''}}{\sqrt{\boldsymbol{R'}\cdot\boldsymbol{R'}}} - \frac{(\boldsymbol{R'}\cdot\boldsymbol{R''})\boldsymbol{R'}}{(\boldsymbol{R'}\cdot\boldsymbol{R'})\sqrt{\boldsymbol{R'}\cdot\boldsymbol{R'}}}. \tag{18}$$

Note that the normal $\boldsymbol{n}$ here is not a unit vector.

For convenience, a new vector $\boldsymbol{\tau}$ is specified as

$$\boldsymbol{\tau} = \frac{\boldsymbol{R''}}{\sqrt{\boldsymbol{R'} \cdot \boldsymbol{R'}}}, \tag{19}$$

where vectors $\boldsymbol{\tau}$ and $\boldsymbol{R''}$ have the identical direction.

Therefore, Eq. (18) could be rewritten as

$$\boldsymbol{n} = \boldsymbol{\tau} - (\boldsymbol{\tau} \cdot \boldsymbol{t})\boldsymbol{t}. \tag{20}$$

Likewise, the governing equation Eq. (13) of the system could be rewritten as

$$m\ddot{\boldsymbol{R}} - EA(\boldsymbol{\tau} \cdot \boldsymbol{t})\boldsymbol{t} - EA(\sqrt{\boldsymbol{R'} \cdot \boldsymbol{R'}} - 1)\boldsymbol{\tau} = \boldsymbol{P}, \tag{21}$$

or

$$m\ddot{\boldsymbol{R}} + EA\boldsymbol{n} - EA\sqrt{\boldsymbol{R'} \cdot \boldsymbol{R'}}\boldsymbol{\tau} = \boldsymbol{P}. \tag{22}$$

In terms of Eq. (22), there are two terms related to the elasticity of the cable. The two terms are in the direction $\boldsymbol{\tau}$ and normal direction of the cable. In other words, the curved cable will result in an elastic force in the normal direction which is in a linear relationship with the curvature of the cable. Besides, the internal tensile forces of curved cables are not only in the tangent direction but in the direction $\boldsymbol{\tau}$ or normal direction of the cables.

Note that the osculating plane is spanned by the tangent and normal vectors passing through one point on a curve. From Eq. (20), it is found that the vector $\boldsymbol{R''}$ or $\boldsymbol{\tau}$ is embedded in the osculating plane. Consequently, the unit binormal vector $\boldsymbol{b}$ of the curve could be given by

$$\boldsymbol{b} = \frac{\boldsymbol{R'} \times \boldsymbol{R''}}{\sqrt{\boldsymbol{R'} \cdot \boldsymbol{R'}}\sqrt{\boldsymbol{R''} \cdot \boldsymbol{R''}}}, \tag{23}$$

where operator $\times$ means the cross product of two vectors.

To sum up, the local reference frame at a point on the curve is associated with four vectors, i.e. $\boldsymbol{t}$, $\boldsymbol{\tau}$, $\boldsymbol{n}$, and $\boldsymbol{b}$. The four vectors and their relationships are shown in Fig. 2.

According to the derived governing equation, external forces acted along the binormal directions of the curve could not be balanced by the internal elastic

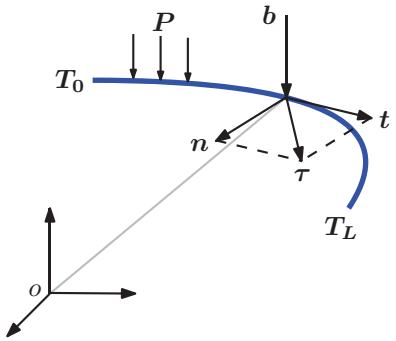

Figure 2: The local reference frame of the curve.

forces of the extended cable, which should only be balanced by the other forces, e. g. the inertia force. This phenomenon is due to the fact that the cable could not bear bending moments.

If the normal vector $\boldsymbol{n}$ is shrunk to zero and $\boldsymbol{R''} \neq \boldsymbol{0}$, we can obtain $\boldsymbol{R''} = \alpha \boldsymbol{R'}$, where α is a constant. This case means that the extensible cable is a straight line, and Eq. (22) will degenerate into the equation of motion of straight bars in vibration mechanics. On the other hand, we can obtain the relationship $\boldsymbol{R''} = \boldsymbol{n}$ if the cable is not extended.

Next, we will consider the boundary conditions of the governing equation shown in Eq. (14). At the two endpoints of the cable, we could specify the geometrical constraints or tensile forces. But it can not be easily realized in the laboratory if we only specify the tensile forces at the two endpoints.

The constructed governing equation is a vector equation which is equivalent to three scalar equations. In addition, we could achieve three different scalar equations in another way.

On dot multiplying Eq. (22) by the tangent $\boldsymbol{t}$, vector $\boldsymbol{R''}$ and binormal $\boldsymbol{b}$, one can obtain

$$m\ddot{\boldsymbol{R}} \cdot \boldsymbol{R'} - EA\boldsymbol{R''} \cdot \boldsymbol{R'} = \boldsymbol{P} \cdot \boldsymbol{R'}, \tag{24}$$

$$m\ddot{\boldsymbol{R}} \cdot \boldsymbol{R''} - EA\frac{(\boldsymbol{R''} \cdot \boldsymbol{R'})^2}{(\sqrt{\boldsymbol{R'} \cdot \boldsymbol{R'}})^3} - EA(\sqrt{\boldsymbol{R'} \cdot \boldsymbol{R'}} - 1)\frac{\boldsymbol{R''} \cdot \boldsymbol{R''}}{\sqrt{\boldsymbol{R'} \cdot \boldsymbol{R'}}} = \boldsymbol{P} \cdot \boldsymbol{R''}, \tag{25}$$

$$m\ddot{\boldsymbol{R}} \cdot \boldsymbol{b} = \boldsymbol{P} \cdot \boldsymbol{b}. \tag{26}$$

The new scalar equations are the component equations of the vector equation along the $\boldsymbol{t}$, $\boldsymbol{\tau}$, and $\boldsymbol{b}$ directions.

It could be viewed here that the external forces acted along the binormal $\boldsymbol{b}$ can not be balanced by the internal elastic force of the cable.

3. Case study

In this section, special mechanical models are studied by using the presented method to assess the developed model.

3.1. Case 1: a cable under a uniformly distributed load in the normal direction

The configuration of the model in this case is depicted as Fig. 3.

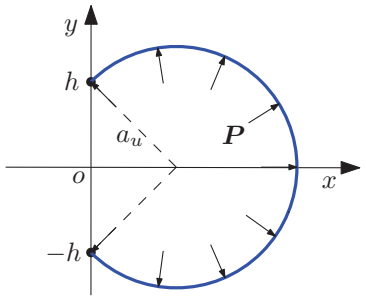

Figure 3: A cable under a uniformly distributed load in the normal direction.

Assume that the cable is located in xy plane of the Cartesian coordinate system. The two endpoints of the extensible cable are fixed whose coordinates are $(0, -h)$ and $(0, h)$. A uniformly distributed load $\boldsymbol{P}$ is perpendicularly acted on the cable. The length L of the cable is greater than $2h$, which ensures that there is no pre–strain in the cable. Constants E and A are the elastic modulus and cross-sectional area of the cable.

The inertia force is neglected in the model. In consequence, the governing equation could be formulated as

$$EA\boldsymbol{n} - EA\sqrt{\boldsymbol{R}' \cdot \boldsymbol{R}'}\boldsymbol{\tau} = -P\frac{\boldsymbol{n}}{\sqrt{\boldsymbol{n} \cdot \boldsymbol{n}}}. \tag{27}$$

Note that the unit direction vector of the distributed load $\boldsymbol{P}$ is $-\boldsymbol{n}/\sqrt{\boldsymbol{n} \cdot \boldsymbol{n}}$.

To begin with, dot multiplying both hand sides of the governing equation with vector $\boldsymbol{t}$, one can obtain

$$-EA\sqrt{\boldsymbol{R'}\cdot\boldsymbol{R'}}\boldsymbol{\tau}\cdot\boldsymbol{t}=0. \tag{28}$$

That is to say,

$$\boldsymbol{n}=\boldsymbol{\tau}. \tag{29}$$

Further, inserting Eq. (29) into Eq. (27) one can simplify the governing equation as

$$\left\{EA(\sqrt{\boldsymbol{R'}\cdot\boldsymbol{R'}}-1)-\frac{P}{\sqrt{\boldsymbol{n}\cdot\boldsymbol{n}}}\right\}\boldsymbol{n}=\boldsymbol{0}. \tag{30}$$

As stated above, the cable will be a straight line if $\boldsymbol{n}=\boldsymbol{0}$. Obviously it is not the solution we seek.

Therefore, the solution of the governing equation is given by

$$EA(\sqrt{\boldsymbol{R'}\cdot\boldsymbol{R'}}-1)=\frac{P}{\sqrt{\boldsymbol{n}\cdot\boldsymbol{n}}}. \tag{31}$$

In addition, from Eq. (29) one can find

$$(\sqrt{\boldsymbol{R'}\cdot\boldsymbol{R'}})'=\frac{\boldsymbol{R'}\cdot\boldsymbol{R''}}{\sqrt{\boldsymbol{R'}\cdot\boldsymbol{R'}}}=0, \tag{32}$$

which means term $\sqrt{\boldsymbol{R'}\cdot\boldsymbol{R'}}$ is a constant. According to Eq. (31), an important result is achieved that the term $\sqrt{\boldsymbol{n}\cdot\boldsymbol{n}}$ is a constant as well. Moreover, the internal elastic force of the cable is also a constant at different positions in this model.

Thus, Eq. (31) could be rewritten as

$$\sqrt{\boldsymbol{R'}\cdot\boldsymbol{R'}}=1+\frac{Pa}{EA}, \tag{33}$$

where $a=1/\sqrt{\boldsymbol{n}\cdot\boldsymbol{n}}$.

By the way, the length L_e of the elongated cable is given by

$$L_e=\int_0^L\sqrt{\boldsymbol{R'}\cdot\boldsymbol{R'}}ds=(1+\frac{Pa}{EA})L. \tag{34}$$

Here a new variable is induced by the definition

$$u=s\sqrt{\boldsymbol{R'}\cdot\boldsymbol{R'}}=s(1+\frac{Pa}{EA}). \tag{35}$$

According to Eq. (33), one can obtain

$$\frac{\partial \boldsymbol{R}}{\partial u} \cdot \frac{\partial \boldsymbol{R}}{\partial u} = 1. \tag{36}$$

The boundary conditions expressed by variable u in the Cartesian coordinate system are given by

$$x(0) = 0,\ x(L + \frac{Pa}{EA}L) = 0,\ y(0) = -h,\ y(L + \frac{Pa}{EA}L) = h. \tag{37}$$

Note that the variable s and u are the Lagrange and Euler coordinates to depict the identical mechanical model. Next, the radius a_u of curvature could be expressed as

$$\frac{1}{a_u} = \sqrt{\frac{\partial^2 \boldsymbol{R}}{\partial u^2} \cdot \frac{\partial^2 \boldsymbol{R}}{\partial u^2}} = \frac{1}{a\sqrt{\boldsymbol{R'} \cdot \boldsymbol{R'}}}, \tag{38}$$

which shows the relationship between the radius a_u of curvature and the constant a. Meanwhile, the radius a_u of curvature is a constant and the solution curve of this case is a circle.

Further, in terms of the geometrical configuration of the system, radius a_u of the circle could be figured out by the equation

$$\frac{h}{a_u} = \sin \frac{(1 + \frac{Pa}{EA})L}{2a_u}, \tag{39}$$

where $a_u > 0$.

By the combination of Eqs. (38) and (39), the radius a_u of curvature of the cable could be obtained numerically.

In terms of the boundary conditions, the solution of the system could be formulated as

$$\boldsymbol{R}(u) = \pm \left\{ a_u \cos(\frac{u}{a_u} + \phi) + x_0 \right\} \mathbf{e}_x + \left\{ a_u \sin(\frac{u}{a_u} + \phi) \right\} \mathbf{e}_y, \tag{40}$$

where ϕ and x_0 are given by

$$\phi = -\arcsin \frac{h}{a_u}, \quad x_0 = -a_u \cos \arcsin \frac{h}{a_u}. \tag{41}$$

Until now, the solution of this mechanical model is achieved in theory. The main concern of the model is to solve Eq. (39) and find the radius a_u of the solution curve. This equation is a transcendental equation which could be resolved by means of numerical methods.

For instance, assumed that $h = 0.5$ m and $L = 2.0$ m, the numerical solutions of radius a_u of the circle are 0.5386 m and 0.5499 m for the cases of $P/EA = 0.1$ m^{-1}and $P/EA = 0.2$ m^{-1} approximately. In addition, a_u and a equal 0.5276 m if $P/EA = 0.0$ m^{-1}. This case represents the initial geometrical configuration of the system.

Next, let $a = a_u$ in Eq. (39). The numerical results of the constant a are 0.5392 m, 0.5525 m and 0.5276 m corresponding to the cases of $P/EA = 0.1$ m^{-1}, 0.2 m^{-1} and 0.0 m^{-1}. It is elucidated that the constant a could be used to approximate to the radius of curvature of the cable if its elongation is a small quantity. Hence, in Eq. (33) there is an anti-proportional relationship between the radius of curvature and the normal load, if the internal elastic force of the cable keeps unchanged.

3.2. Case 2: a cable under a uniformly distributed load in an identical direction

The configuration of the case is shown in Fig. 4. The model is similar with the previous case except that the uniformly distributed load is acted on the cable in the x direction.

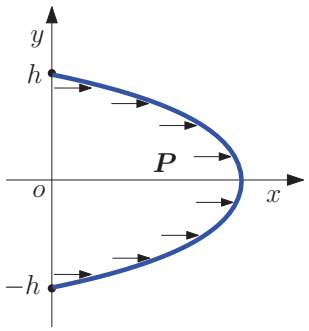

Figure 4: A cable under a uniformly distributed load in the x direction.

The governing equation of this model could be formulated as

$$EA\boldsymbol{n} - EA\sqrt{\boldsymbol{R}' \cdot \boldsymbol{R}'}\boldsymbol{\tau} = P\mathbf{e}_x, \tag{42}$$

where the position vector of a point on the cable is given by

$$\boldsymbol{R}(s) = x(s)\mathbf{e}_x + y(s)\mathbf{e}_y. \tag{43}$$

Further, the tangent $\boldsymbol{t}$, normal $\boldsymbol{n}$ and vector $\boldsymbol{\tau}$ are read as

$$\boldsymbol{t} = \frac{x'\mathbf{e}_x + y'\mathbf{e}_y}{\sqrt{x'^2 + y'^2}}, \tag{44}$$

$$\boldsymbol{n} = \frac{x''\mathbf{e}_x + y''\mathbf{e}_y}{\sqrt{x'^2 + y'^2}} - \frac{(x'x'' + y'y'')(x'\mathbf{e}_x + y'\mathbf{e}_y)}{(\sqrt{x'^2 + y'^2})^3}, \tag{45}$$

$$\boldsymbol{\tau} = \frac{x''\mathbf{e}_x + y''\mathbf{e}_y}{\sqrt{x'^2 + y'^2}}. \tag{46}$$

On dot multiplying the governing equation by the tangent $\boldsymbol{t}$, one can obtain

$$x'x'' + y'y'' = -\frac{P}{EA}x'. \tag{47}$$

Inserting Eq. (47) into the governing equation, we could obtain the component equations as

$$x'' = \frac{P}{EA}\frac{\dfrac{x'x'}{x'^2 + y'^2} - \sqrt{x'^2 + y'^2}}{\sqrt{x'^2 + y'^2} - 1}, \tag{48}$$

$$y'' = \frac{P}{EA}\frac{\dfrac{x'y'}{x'^2 + y'^2}}{\sqrt{x'^2 + y'^2} - 1}. \tag{49}$$

Moreover, the corresponding boundary conditions are given by

$$x(0) = 0, x(L) = 0, y(0) = -h, y(L) = h. \tag{50}$$

The governing equation and boundary conditions are categorized into the two–point boundary value problem, which could be solved numerically by using the shooting method[34]. The boundary value problem is restated to an initial value problem of ordinary differential equations. Then the task is to find appropriate initial values whereby the original boundary conditions are met under a tolerance error.

In the work, the derivatives $x'(0)$ and $y'(0)$ are treated as part of the initial conditions. By an iterative procedure, the values $x'(0)$ and $y'(0)$ could be determined to ensure that the boundary values $x(L)$ and $y(L)$ are satisfied.

The mechanical parameters used in numerical computation are specified as the following: $h = 0.5$ m, $L = 2.0$ m. The tolerance error of boundary conditions

is set to 0.001 m. Note that the strain ϵ could be used to evaluate the internal tensile force of the cable.

The numerical examples of the considered model are shown in Tab. 1. The initial values $x'(0)$ and $y'(0)$ are given corresponding to different parameters P/EA. Note that L_e is the length of the elongated cable. Further, the cable is elongated more with the external load increasing.

Table 1: The numerical examples of cables under distributed loads in x direction.

$P/EA(\mathrm{m}^{-1})$	$x'(0)$	$y'(0)$	L_e (m)
0.05	1.02644	0.22677	2.09867
0.10	1.07804	0.22950	2.15655
0.20	1.18080	0.23434	2.27037

The contours and strain distributions of the cables are illustrated in Figs. 5 and 6, where parameter $P/EA = 0.05$ m^{-1}, 0.10 m^{-1} and 0.20 m^{-1}. It can be found that the two curves are symmetrically located in the arc ranges $(0,\ L/2)$ and $(L/2, L)$.

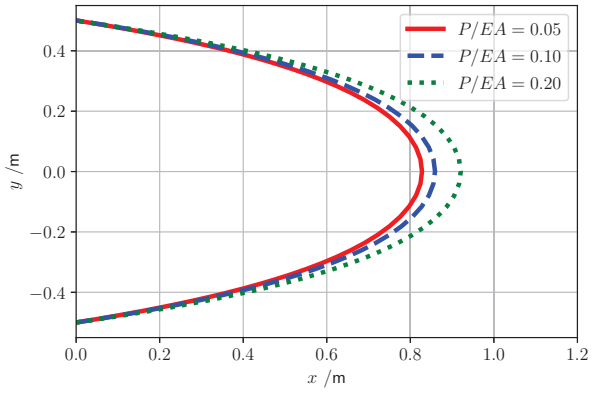

Figure 5: The contours of cables when $P/EA = 0.05$ m^{-1}, 0.10 m^{-1} and 0.20 m^{-1}.

In the figures, the contour of the cable will enlarge if the external load increases, and the internal tensile force of the cable will grow as well. The maximum values of the internal force are located at the two endpoints of the cables

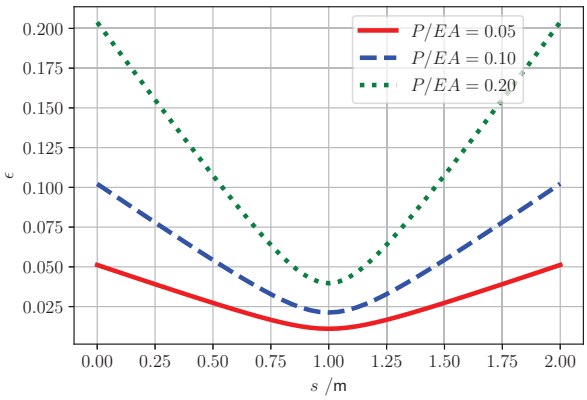

Figure 6: The strain distributions of cables when $P/EA = 0.05$ m^{-1}, 0.10 m^{-1} and 0.20 m^{-1}.

while the minimum values are at the position $s = L/2$. Meanwhile, the maximum value of the tensile force at either of the two endpoints is approximately equal to $PL/2$, which indicates that the total external force is evenly acted on the two endpoints. Further, the internal forces of the cables are varying in a linear relationship with the arc lengths in the two half cables.

3.3. Case 3: a sagged cable under its self-weight

In the case, a cable subject to the gravitational force is investigated. That means the gravitational potential energy should be considered in the model. The gravitational potential energy U_g could be formulated as

$$U_g = -\int_0^L mg\boldsymbol{R}(s) \cdot \mathbf{e}_g ds, \tag{51}$$

where $\mathbf{e}_g$ is the unit vector in the direction of gravity and g denotes the gravity acceleration.

The variation of the gravitational potential energy is given by

$$\int_{t0}^{t1} \delta U_g dt = \int_{t0}^{t1} \delta(\int_0^L -mg\boldsymbol{R}(s) \cdot \mathbf{e}_g ds)dt = \int_{t0}^{t1}\int_0^L -mg\mathbf{e}_g \cdot \delta\boldsymbol{R}(s)dsdt. \tag{52}$$

Inserting the variation of the gravitational potential energy into Eq. (10) to compose the variation of the total potential energy, we could achieve the

governing equation in this case as

$$m\ddot{\boldsymbol{R}} - EA(\boldsymbol{\tau}\cdot\boldsymbol{t})\boldsymbol{t} - EA(\sqrt{\boldsymbol{R}'\cdot\boldsymbol{R}'}-1)\boldsymbol{\tau} - mg\mathbf{e}_g = \boldsymbol{P}. \tag{53}$$

In addition, the boundary conditions of the case are unaltered as shown in Eq. (14).

According to the derived governing equation and boundary conditions, there is little discrepancy between the models with and without the gravitational potential energy.

The configuration of the model considering the gravitational potential energy is shown in Fig. 7. A cable only subject to the gravitational force is sagged in three–dimensional space. The unit vector $\mathbf{e}_g$ (direction of gravity) coincides with the direction $\mathbf{e}_x$. The coordinates of two endpoints of the cable are $(0, -h, 0)$ and $(d, h, 0)$. Note that this case is similar to case 2, except that the two endpoints are not located in an identical horizontal plane.

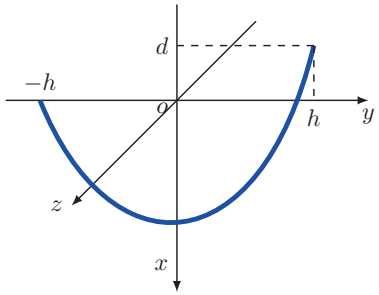

Figure 7: A sagged cable under its self–weight.

Likewise, inertia forces are omitted and the governing equation could be simplified as

$$EA\boldsymbol{n} - EA\sqrt{\boldsymbol{R}'\cdot\boldsymbol{R}'}\boldsymbol{\tau} = mg\mathbf{e}_x. \tag{54}$$

Here we would like to manifest that the model in the case is a planar curve.

In three–dimensional space, assume that the binormal $\boldsymbol{b}$ of the cable is not a constant vector. On dot multiplying the governing equation with the binormal $\boldsymbol{b}$, we could obtain the relationship $\boldsymbol{b}\cdot\mathbf{e}_x = 0$. By differentiating the relationship with respect to the arc length, we could reach $\boldsymbol{b}'\cdot\mathbf{e}_x = 0$. Because the binormal

$\boldsymbol{b}$ is a unit vector, the relationship $\boldsymbol{b} \cdot \boldsymbol{b}' = 0$ could be derived. Here the vector $\boldsymbol{b}'$ is parallel to the normal $\boldsymbol{n}$. Finally, we could conclude that the tangent $\boldsymbol{t}$ is also parallel to the vector $\mathbf{e}_x$, which implies that the cable is a straight line. On the other hand, this is not in agreement with the configuration of this case. Therefore, we can draw the conclusion that the binormal $\boldsymbol{b}$ in this case is a constant vector. That is to say, the cable of this case is a planar curve.

Let $P = mg$ and the component governing equations of this case are given by Eqs. (48) and (49).

Moreover, the boundary conditions of the case are given by

$$x(0) = 0, x(L) = d, y(0) = -h, y(L) = h. \tag{55}$$

Note that parameter d denotes the altitude difference of the two endpoints.

The mechanical parameters of this case are specified as the following: $h =$ 0.5 m, $L = 2.0$ m. The tolerance error of boundary conditions is set to 0.001 m.

The numerical examples of this case are shown in Tab. 2, where the different parameters d and mg/EA are considered. Note that the cable will elongate more if the altitude difference d of two endpoints increases.

Table 2: The numerical examples of cables under self–weight.

d (m)	mg/EA (m^{-1})	$x'(0)$	$y'(0)$	L_e (m)
-0.1	0.05	1.02168	0.23707	2.09878
	0.10	1.07132	0.23910	2.15676
-0.3	0.05	1.01052	0.26270	2.09977
	0.10	1.05656	0.26256	2.15856

The cable contours and strain distributions of the numerical examples are illustrated in Figs. 8, 9, 10, and 11.

According to the figures, the altitude difference of two endpoints will result in the discrepancy of their tensile forces. And the discrepancy of tensile forces at two endpoints grows with the altitude difference increasing. The tensile force at the high endpoint is greater than half self–weight of the cable while the tensile force is opposite at the low endpoint.

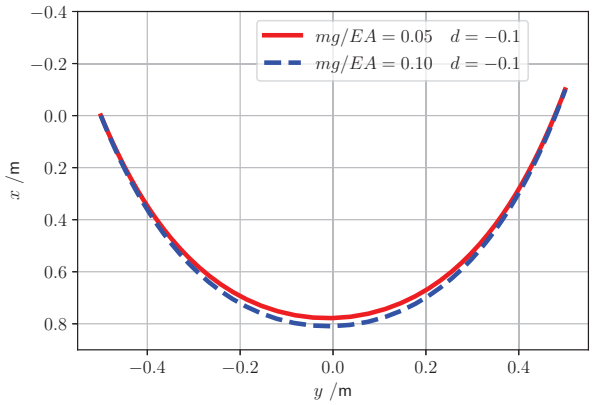

Figure 8: The contours of cables when $d = -0.1$ m and $mg/EA = 0.05$ m^{-1} and 0.10 m^{-1}.

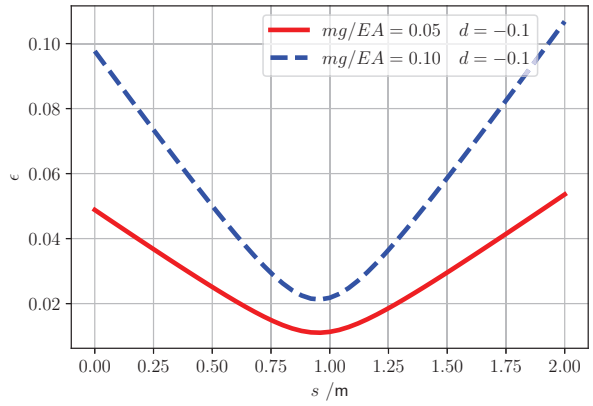

Figure 9: The strain distributions of cables when $d = -0.1$ m and $mg/EA = 0.05$ m^{-1} and 0.10 m^{-1}.

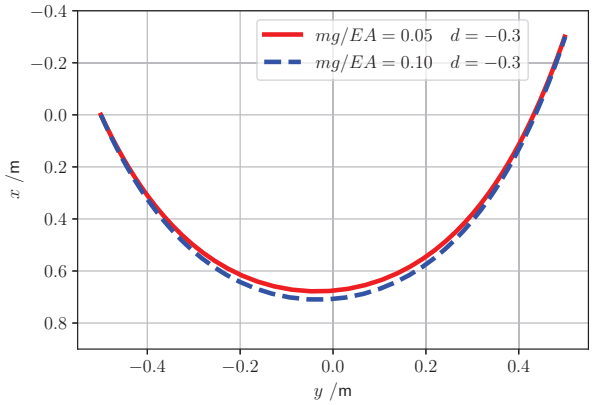

Figure 10: The contours of cables when $d = -0.3$ m and $mg/EA = 0.05$ m^{-1} and 0.10 m^{-1}.

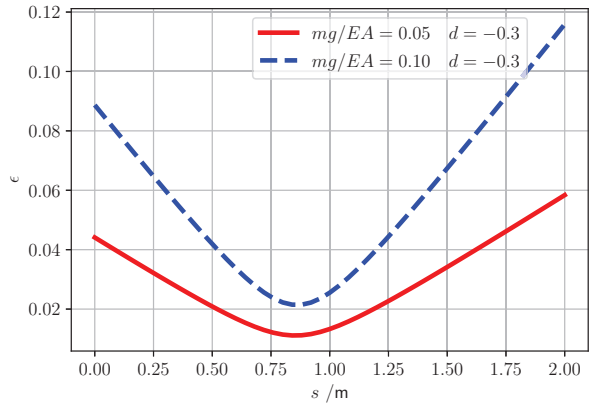

Figure 11: The strain distributions of cables when $d = -0.3$ m and $mg/EA = 0.05$ m^{-1} and 0.10 m^{-1}.

4. Evaluation of the method

In this section, the presented model will be evaluated by using the experimental results available in published literature. Dreyer and Vuuren[35] studied the continuous and discrete models of cables with bending stiffness in static situations, and those models are assessed by using physical experiments. The experiments on a sagged cable under self-weight were conducted(see Fig. 7), and the coordinates of specified points on the cable were shown in that work.

The ragged cable is anchored at two points in the xy plane of the Cartesian coordinate system. The coordinates of the two points are (0, 0) and $(x(L), y(L))$ where L means the length of the cable.

The physical parameters of the cable are specified as follows: $L = 4.13$ m, $EA = 3.927$e6 N, $m = 0.225$ kg/m. Accordingly, we could obtain $mg/EA =$ 5.615e-7 1/m. The tolerance error of numerical computations is set to 0.01 m. Considering different positions of final endpoints, the numerical and experimental results of coordinates of specified points on the cable are shown in Tabs. 3, 4, and 5. Note that $\bar{x}(s)$ and $\bar{y}(s)$ denote the experimental data of positions of the specified points on the cable.

By comparison, it is viewed that the numerical results based on the presented model agree well with the experimental data of discrete points on the cable.

In this work, bending stiffness of cables is not considered in the theoretical modeling, but it exists in practice. We deem that the bending stiffness of cables is a factor leading to the discrepancy between the numerical and experimental data.

5. Conclusions

In the work, attention is paid to a fundamental mechanic model. The authors would like to develop a theoretical model and study the dynamic behavior of non-prestrained cables under external forces. In the linear elastic range, the model is formulated in terms of the Hamilton's principle. According to the vari-

Table 3: Comparison of numerical and experimental results when $x(L) = 0.0$ m and $y(L) = 3.5$ m. (m)

s	$x(s)$	$y(s)$	$\bar{x}(s)$	$\bar{y}(s)$
0.00	0.000	0.000	0.000	0.000
0.41	0.300	0.279	0.291	0.292
0.83	0.569	0.600	0.559	0.612
1.24	0.780	0.952	0.789	0.956
1.65	0.919	1.337	0.926	1.340
2.07	0.968	1.753	0.993	1.757
2.48	0.918	2.159	0.926	2.160
2.89	0.779	2.544	0.797	2.549
3.30	0.569	2.896	0.559	2.888
3.72	0.301	3.219	0.296	3.209
4.13	0.003	3.500	0.000	3.500

Table 4: Comparison of numerical and experimental results when $x(L) = 0.1$ m and $y(L) = 3.5$ m. (m)

s	$x(s)$	$y(s)$	$\bar{x}(s)$	$\bar{y}(s)$
0.00	0.000	0.000	0.000	0.000
0.41	0.305	0.273	0.290	0.283
0.83	0.583	0.588	0.582	0.596
1.24	0.804	0.933	0.813	0.934
1.65	0.956	1.313	0.973	1.314
2.07	1.020	1.727	1.039	1.728
2.48	0.985	2.134	1.001	2.138
2.89	0.857	2.523	0.870	2.534
3.30	0.656	2.880	0.659	2.878
3.72	0.394	3.208	0.388	3.201
4.13	0.100	3.493	0.100	3.500

Table 5: Comparison of numerical and experimental results when $x(L) = -0.88$ m and $y(L) = 3.36$ m. (m)

s	$x(s)$	$y(s)$	$\bar{x}(s)$	$\bar{y}(s)$
0.00	0.000	0.000	0.000	0.000
0.41	0.263	0.314	0.218	0.347
0.83	0.472	0.677	0.413	0.722
1.24	0.592	1.068	0.545	1.110
1.65	0.608	1.477	0.590	1.508
2.07	0.515	1.885	0.532	1.936
2.48	0.334	2.252	0.376	2.316
2.89	0.087	2.579	0.134	2.646
3.30	-0.204	2.867	-0.170	2.922
3.72	-0.533	3.127	-0.521	3.154
4.13	-0.876	3.353	-0.880	3.360

ation of the action integral, the governing equation and corresponding boundary conditions are achieved.

The local reference frame of spatial curves is analyzed, which is associated with four vectors. It is viewed that the external force along the binormal direction could not be balanced by the internal elastic force of the cable itself. And elastic forces in the normal directions are generated by the curvature of the cable. Applications of the presented method are given and the results are reasonable. The developed model is evaluated by experimental data in published literature, and the numerical results based on the presented approach agree well with the experimental data. In addition, the developed model could provide support to the modeling of membranes.

Declaration of interest

The authors declare that they have no conflict of interest.

Acknowledgments

This work was supported by National Key Research and Development Program of China (No. 2018YFB1105304) and China Postdoctoral Science Foundation (No. 2013M542306). The authors greatly appreciate the financial support for this work.

References

[1] N. C. Perkins, C. D. Mote, Three–dimensional vibration of travelling elastic cables, Journal of Sound and Vibration 114 (2) (1987) 325–340. doi:10.1016/S0022-460X(87)80157-8.

[2] C. L. Lee, N. C. Perkins, Nonlinear oscillations of suspended cables containing a two-to-one internal resonance, Nonlinear Dynamics 3 (6) (1992) 465–490. doi:10.1007/BF00045648.

[3] A. Luongo, G. Piccardo, Non–linear galloping of sagged cables in 1:2 internal resonance, Journal of Sound and Vibration 214 (5) (1998) 915–940. doi:10.1006/jsvi.1998.1583.

[4] G. Rega, Nonlinear vibrations of suspended cables—Part I: Modeling and analysis, Applied Mechanics Reviews 57 (6) (2004) 443–478. doi:10.1115/1.1777224.

[5] A. Luongo, D. Zulli, G. Piccardo, A linear curved-beam model for the analysis of galloping in suspended cables, Journal of Mechanics of Materials and Structures 2 (4) (2007) 675–694. doi:10.2140/jomms.2007.2.675.

[6] H. J. Kang, T. D. Guo, Y. Y. Zhao, W. B. Fu, L. H. Wang, Dynamic modeling and in-plane 1:1:1 internal resonance analysis of cable-stayed bridge, European Journal of Mechanics - A/Solids 62 (2017) 94–109. doi:10.1016/j.euromechsol.2016.10.016.

[7] S. K. Hashemi, M. A. Bradford, H. R. Valipour, Dynamic response of cable-stayed bridge under blast load, Engineering Structures 127 (2016) 719–736. doi:10.1016/j.engstruct.2016.08.038.

[8] M. T. Song, D. Q. Cao, W. D. Zhu, Q. S. Bi, Dynamic response of a cable-stayed bridge subjected to a moving vehicle load, Acta Mechanica 227 (10) (2016) 2925–2945. doi:10.1007/s00707-016-1635-0.

[9] G. Xie, J. Yin, R. Liu, B. Chen, D. Cai, Experimental and numerical investigation on the static and dynamic behaviors of cable-stayed bridges with CFRP cables, Composites Part B: Engineering 111 (2017) 235–242. doi:10.1016/j.compositesb.2016.11.048.

[10] Q. Han, J. Wen, X. Du, Z. Zhong, H. Hao, Nonlinear seismic response of a base isolated single pylon cable-stayed bridge, Engineering Structures 175 (2018) 806–821. doi:10.1016/j.engstruct.2018.08.077.

[11] A. Javanmardi, Z. Ibrahim, K. Ghaedi, M. Jameel, H. Khatibi, M. Suhatril, Seismic response characteristics of a base isolated cable-stayed bridge under moderate and strong ground motions, Archives of Civil and Mechanical Engineering 17 (2) (2017) 419–432. doi:10.1016/j.acme.2016.12.002.

[12] M. Lepidi, V. Gattulli, Static and dynamic response of elastic suspended cables with thermal effects, International Journal of Solids and Structures 49 (9) (2012) 1103–1116. doi:10.1016/j.ijsolstr.2012.01.008.

[13] L. Wang, Y. Wu, D. Wang, Thermal effect on damaged stay-cables, Journal of Theoretical and Applied Mechanics 52 (4) (2014) 1071–1082–1082. doi:10.15632/jtam-pl.52.4.1071.

[14] F. Treyssède, Finite element modeling of temperature load effects on the vibration of local modes in multi-cable structures, Journal of Sound and Vibration 413 (2018) 191–204. doi:10.1016/j.jsv.2017.10.022.

[15] M. Wei, K. Lin, L. Jin, D. Zou, Nonlinear dynamics of a cable-stayed beam driven by sub-harmonic and principal parametric resonance, Inter-

national Journal of Mechanical Sciences 110 (2016) 78–93. doi:10.1016/j.ijmecsci.2016.03.007.

[16] Y. Song, Z. Liu, H. Wang, X. Lu, J. Zhang, Nonlinear analysis of wind-induced vibration of high-speed railway catenary and its influence on pantograph-catenary interaction, Vehicle System Dynamics 54 (6) (2016) 723–747. doi:10.1080/00423114.2016.1156134.

[17] P. Antunes, J. Ambrósio, J. Pombo, A. Facchinetti, A new methodology to study the pantograph–catenary dynamics in curved railway tracks, Vehicle System Dynamics 58 (3) (2020) 425–452. doi:10.1080/00423114.2019.1583348.

[18] S. Gregori, M. Tur, E. Nadal, J. Aguado, F. Fuenmayor, F. Chinesta, Fast simulation of the pantograph–catenary dynamic interaction, Finite Elements in Analysis and Design 129 (2017) 1–13. doi:10.1016/j.finel.2017.01.007.

[19] S. Gregori, M. Tur, A. Pedrosa, J. E. Tarancón, F. J. Fuenmayor, A modal coordinate catenary model for the real-time simulation of the pantograph-catenary dynamic interaction, Finite Elements in Analysis and Design 162 (2019) 1–12. doi:10.1016/j.finel.2019.05.001.

[20] Y. Song, H. Ouyang, Z. Liu, G. Mei, H. Wang, X. Lu, Active control of contact force for high-speed railway pantograph-catenary based on multi-body pantograph model, Mechanism and Machine Theory 115 (2017) 35–59. doi:10.1016/j.mechmachtheory.2017.04.014.

[21] P. Nåvik, A. Rønnquist, S. Stichel, Variation in predicting pantograph-catenary interaction contact forces, numerical simulations and field measurements, Vehicle System Dynamics 55 (9) (2017) 1265–1282. doi:10.1080/00423114.2017.1308523.

[22] Y. Song, Z. Liu, F. Duan, Z. Xu, X. Lu, Wave propagation analysis in high-speed railway catenary system subjected to a moving pantograph, Applied

Mathematical Modelling 59 (2018) 20–38. doi:10.1016/j.apm.2018.01.001.

[23] Y. Song, Z. Liu, H. Wang, X. Lu, J. Zhang, Nonlinear modelling of high-speed catenary based on analytical expressions of cable and truss elements, Vehicle System Dynamics 53 (10) (2015) 1455–1479. doi:10.1080/00423114.2015.1051548.

[24] T. Guo, H. Kang, L. Wang, Y. Zhao, An asymptotic expansion of cable-flexible support coupled nonlinear vibrations using boundary modulations, Nonlinear Dynamics 88 (1) (2017) 33–59. doi:10.1007/s11071-016-3229-8.

[25] T. Guo, H. Kang, L. Wang, Y. Zhao, An inclined cable excited by a non-ideal massive moving deck: An asymptotic formulation, Nonlinear Dynamics 95 (1) (2019) 749–767. doi:10.1007/s11071-018-4594-2.

[26] V. Gattulli, M. Lepidi, F. Potenza, U. Di Sabatino, Dynamics of masonry walls connected by a vibrating cable in a historic structure, Meccanica 51 (11) (2016) 2813–2826. doi:10.1007/s11012-016-0509-9.

[27] V. Gattulli, M. Lepidi, F. Potenza, U. Di Sabatino, Modal interactions in the nonlinear dynamics of a beam-cable-beam, Nonlinear Dynamics 96 (4) (2019) 2547–2566. doi:10.1007/s11071-019-04940-8.

[28] W. B. Fraser, On the theory of ring spinning, Philosophical Transactions of the Royal Society of London. Series A: Physical and Engineering Sciences 342 (1665) (1993) 439–468. doi:10/cj9vmw.

[29] H. B. Tang, B. G. Xu, X. M. Tao, J. Feng, Mathematical modeling and numerical simulation of yarn behavior in a modified ring spinning system, Applied Mathematical Modelling 35 (1) (2011) 139–151. doi:10.1016/j.apm.2010.05.013.

[30] R. Yin, X. M. Tao, B. G. Xu, Mathematical modeling of yarn dynamics in a generalized twisting system, Scientific Reports 6 (1) (2016) 24432. doi:10/f8jgzj.

[31] M. Hossain, C. Telke, A. Abdkader, C. Cherif, M. Beitelschmidt, Mathematical modeling of the dynamic yarn path depending on spindle speed in a ring spinning process, Textile Research Journal 86 (11) (2016) 1180–1190. doi:10/f8wpw4.

[32] B. G. Xu, X. M. Tao, Integrated approach to dynamic analysis of yarn twist distribution in rotor spinning: Part I: Steady state, Textile Research Journal 73 (1) (2003) 79–89. doi:10/ddf3ch.

[33] M. P. D. Carmo, Differential Geometry of Curves and Surfaces, 1st Edition, Prentice-Hall, Englewood Cliffs, N.J, 1976.

[34] J. Stoer, R. Bulirsch, Introduction to Numerical Analysis, Springer New York, New York, NY, 2002. doi:10.1007/978-0-387-21738-3.

[35] T. P. Dreyer, J. H. Van Vuuren, A comparison between continuous and discrete modelling of cables with bending stiffness, Applied Mathematical Modelling 23 (7) (1999) 527–541. doi:10.1016/S0307-904X(98)10097-5.